SAND2015-1719J

Effects of repetitive pulsing on multi-kHz planar laser-induced incandescence imaging in laminar and turbulent flames

James B. Michael,[1,*] Prabhakar Venkateswaran,[1,*] Christopher R. Shaddix,[2] and Terrence R. Meyer[1,†]

[1] *Department of Mechanical Engineering, Iowa State University, 2025 Black Engineering, Ames, IA 50011, USA*

[2] *Combustion Research Facility, Sandia National Laboratories, Livermore, CA*

Abstract

Planar laser-induced incandescence (LII) imaging is reported at repetition rates up to 100 kHz using a burst-mode laser system to enable studies of soot formation dynamics in highly turbulent flames. To quantify the accuracy and uncertainty of relative soot volume fraction measurements, the temporal evolution of the LII field in laminar and turbulent flames is examined at various laser operating conditions. Under high-speed repetitive probing, it is found that LII signals are sensitive to changes in soot physical characteristics when operating at high laser fluences within the soot vaporization regime. For these laser conditions, strong planar LII signals are observed at measurement rates up to 100 kHz but are primarily useful for qualitative tracking of soot structure dynamics. However, LII signals collected at lower fluences allow sequential planar measurements of the relative soot volume fraction with sufficient signal-to-noise ratio at repetition rates of 10–50 kHz. Guidelines for identifying and avoiding the onset of repetitive probe effects in the LII signals are discussed, along with other potential sources of measurement error and uncertainty.

OCIS codes: (120.0120) Instrumentation, measurement, and metrology; (120.1740) Combustion diagnostics.

http://dx.doi.org/10.1364/XX.99.099999

* Equal contributions to manuscript

† trm@iastate.edu

1. Introduction

Devices such as aircraft engines and diesel engines produce particulates, such as soot, which are byproducts of the combustion process and are known to be harmful to human health and the environment [1]. In recent years, substantial progress has been made in reducing soot emissions from land-based vehicles by optimizing the combustion process using advanced fuel injection [2, 3] and exhaust-gas recirculation strategies [4] in concert with multifunctional exhaust after-treatment systems [5]. On the other hand, aircraft gas-turbine engines must rely exclusively on optimization of the combustion process for reduction of particulate emissions [6].

In both ground-based and aircraft transportation systems a fundamental understanding of the pollutant formation processes, culminating in validated chemical kinetic models describing the soot formation process, is critical for the development of robust pollutant mitigation strategies [7]. While significant progress has been made in both chemical kinetics and fluid-chemistry interactions, there is still a need to extend existing simulations of sooting behavior to describe the interplay between soot chemistry and the highly unsteady, turbulent flow field seen in practical engine conditions [8, 9]. Doing so requires the improvement and validation of numerical models utilizing high-quality experimental databases. In particular, because of the highly dynamic nature of the turbulence-chemistry interactions and the intermittent nature of soot structure formation in practical combustors, spatio-temporally resolved experimental data are required to accurately capture time dynamics and benchmark numerical simulations. For example, Shaddix *et al.* found that soot production increased fourfold for a flickering methane/air flame as compared with a steady flame at the same mean fuel flow velocity[10]. Temporally and spatially resolved data are needed that can contribute to the validation of direct numerical simulation studies that capture the effects of local curvature, strain, and the duration of interaction between flow structures and flames on soot formation and evolution in turbulent nonpremixed flames [8, 11].

For the measurement of soot volume fraction, laser-induced incandescence (LII) has been developed into a powerful experimental technique that allows measurements with high temporal and spatial resolution. LII involves heating of the soot particles with a high intensity laser pulse and subsequently measuring the emitted radiation as the soot particles cool to the local gas temperature. Single shot measurements of soot volume fraction and particle distributions by LII have been made in a variety of laminar and turbulent flames [12]. By utilizing simultaneous extinction measurements and solving a time-dependent energy conservation equation for the soot particle during the heating and subsequent cooling process, the soot volume fraction and primary particle size information can be extracted from the LII signals [13–15]. These heat transfer processes are influenced strongly by the choice of soot physical properties and gas transport properties, which have strong temperature dependencies [16]. For instance, much of the LII modeling must rely on either graphite-based physical properties or directly measured soot physical and optical parameters [17]. In addition to the heat transfer and transport properties, other sources of uncertainty in soot volume fraction and particle size measurements include optical properties and physico-chemical changes in the soot induced by the laser heating [16, 18]. These uncertainties hinder attempts at quantitative comparison between experimental measurements and numerical models.

Because of the potential utility and challenges in making accurate quantitative soot measurements, the literature on the experimental and modeling aspects of LII is quite extensive [16, 19]. With regard to experimental efforts, much work has been done to investigate the sensitivity of the LII data to various parameters such as laser excitation wavelength [20], laser fluence and spatial profile, detected spectral range, delay between excitation and signal collection, and collection gate widths [19]. For instance, a typical result of the variation of the measured LII signal with laser fluence is shown in Fig. 1(a) when a laser with a top-hat spatial profile is utilized [19]. Initially, the signal increases with laser fluence as the soot is heated to higher temperatures. Beyond $\sim$0.2 J/cm^2, the LII signal plateaus as the soot reaches sublimation temperatures and gradually decreases with increasing laser fluence. While this LII fluence response has been attributed to soot vaporization, the threshold of 0.2 J/cm^2 is not a fixed value. It depends on a variety of experimental parameters such as soot temperature, laser wavelength, and laser beam profile, as shown in Fig. 1(b) [19]. Nevertheless, characterizing the onset of the plateau in LII signal for a given set of experimental parameters and operating in a high fluence regime is often attractive because the LII signal is strong and is not as sensitive to laser absorption and shot-to-shot laser energy

variations.

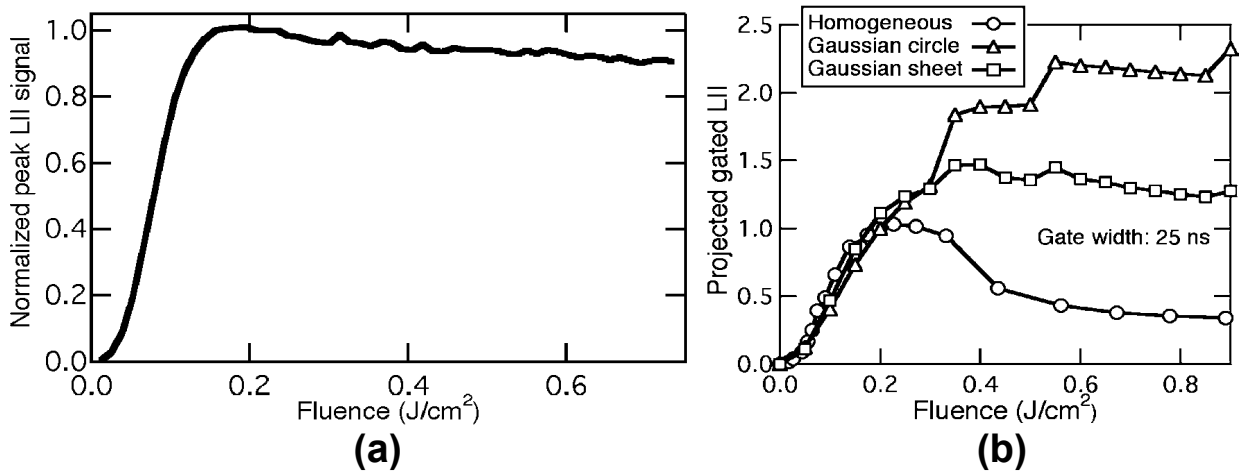

Fig. 1. (a) Variation of LII signal with laser fluence for a top-hat beam profile and (b) dependence of LII signal on laser fluence for different laser beam spatial profiles. Figure reproduced with permission [19].

At high fluences, however, the LII diagnostic technique is no longer non-intrusive since the vaporization process alters the morphology and physical characteristics of the soot particles. For instance, using ex-situ transmission electron microscopy (TEM) measurements, Vander Wal and colleagues showed that pulsed laser heating can have varying degrees of influence on the structural, optical and physical characteristics of the soot particles [21, 22]. At lower fluences, a thermal annealing process was shown to occur without noticeable fragmentation. With increasing laser fluences, evidence of increasing graphitization of the soot and mass loss through vaporization was seen. The observed transformations during both low and high fluence probing indicate the laser heating can alter physical and optical characteristics of the soot on the time-scale of the LII probe duration. The specific problem of vaporization loss during LII laser heating was addressed in work by Witze *et al.* where they found >20% vaporization loss of soot particles at high fluence (>0.2 J/cm^2), but less than 5% loss for fluences below 0.1 J/cm^2 [23].

Extending these measurements to double-pulse experiments, Vander Wal *et al.* demonstrated that, except for very low fluences, the soot signal obtained from the second pulse was lower compared to the signal from the first pulse due to the structural changes and mass loss induced by the first pulse [24]. Thomson *et al.* also investigated the modification of soot particle optical properties by performing simultaneous scattering and extinction studies [17]. They found that there was a gradual decrease in scattering propensity with increasing laser fluence up until the LII signal plateau, where significant mass loss through vaporization occurred. In addition, reversible increases in light absorption were also observed during the time period that the soot was hot, which was attributed to either thermal expansion of the soot particles or a temperature dependent light absorption refractive index function, $E(m_\lambda)$. Permanent increases in $E(m_\lambda)$ ($< 2\%$) were also observed, which were attributed to graphitization of the soot [17]. These experiments suggest that there are temperature-dependent variations of the optical and structural properties of the soot which need to be incorporated into LII models for improved understanding and prediction of LII signals.

With careful evaluation of the soot signal for various laser operating parameters, however, the LII technique can be a powerful tool for investigating the relative distribution of soot volume fraction in a reacting flow field. If the laser fluence is within the low fluence regime, then correction for shot-to-shot laser intensity variations can be performed such that the LII signal is proportional to soot volume fraction to a fair level of certainty so long as the soot size distribution is known. If the laser fluence is within the signal plateau regime, at least for single-shot measurements, the LII signal is at least approximately proportional to the soot volume fraction. Indeed, LII has been used to obtain planar soot distributions in turbulent reacting flow fields in a variety of flame configurations such as jet flames [13, 25, 26], bluff body flames [27] and swirling flames [28, 29].

Much of the work to date has focused on obtaining temporally uncorrelated single-shot LII images. While these data provide valuable insight into the soot distribution within turbulent reacting flow fields, there is still much to be learned about the dynamic nature of the soot formation process and coupling with the turbulent flow field. This requires time-resolved LII measurements where the temporal evolution of the soot structures can be tracked. Franzelli *et al.* recently reported 10 kHz measurements of soot structures with soot scattering simultaneous with polycyclic aromatic hydrocarbon (PAH) and OH fluorescence, but they did not address in detail the potential for quantitative soot volume fraction measurements [30]. There are relatively few reports of high-repetition rate LII studies in which the effects of repetitive pulsing on soot physical characteristics have been evaluated. Sjöholm *et al.* performed time-resolved planar LII using a cluster of Nd:YAG lasers capable of delivering a train of eight pulses with variable pulse separation times [31]. They demonstrated that in a laminar flat flame, the first pulse sublimated the soot particles in the measurement volume resulting in decreased LII signals induced by subsequent probe pulses, consistent with the observations from the double pulse experiments conducted by Vander Wal *et al.* [24]. By varying the time separation between pulses, Sjöholm *et al.* showed that the effects of the initial pulse were present in the LII signal from a second probe pulse for time separations up to 20 ms, which corresponds to the time-scale required to replenish the probe volume with fresh soot via convection [31]. However, when these measurements were extended to turbulent in-cylinder engine conditions, the soot sublimation effects were not observed, perhaps suggesting that laser-affected soot particles were replenished with fresh soot through turbulent mixing. Köhler *et al.* [32] reported planar LII at 3 kHz (along with particle image velocimetry) and noted the possibility of LII signal degradation due to repetitive pulsing, but they did not attempt to quantify or account for these effects. Both inferred gas temperatures from LII measurements and direct measurements suggest that local gas heating effects may be important both in evaluating LII signals and in high speed LII experiments [33, 34]. Recent work by Nordström *et al.* measured local gas temperature rises of ∼100 K, which may be important in modeling LII signal decay in traditional 10 Hz experiments [34]. In high-speed LII measurements, this temperature rise may affect LII signals recorded during repetitive probing.

There is a significant need, therefore, to develop a more thorough understanding of the effects of high-speed, long-term repetitive pulsing on LII signals in dynamic flowfields and under various laser fluences. The goal of this work is to elucidate some of the intrusive effects that repetitive laser pulsing can have on the LII signal and to investigate the conditions under which it may be possible to use this signal for high-speed planar imaging of the soot volume fraction in turbulent flames. This work is enabled by the development and application of burst-mode laser technology [35] which allows high-energy output for 100's and even 1000's of pulse sequences at multi-kHz repetition rates [36–39]. Traditional laser-based diagnostics with high temporal and spatial resolution are unable to achieve the repetition rates necessary to track the time-evolving fluid-flame interactions at high Reynolds numbers [40]. As a result, burst-mode laser systems have found significant use for spectroscopic measurements of minor species and flame-front imaging in turbulent flames [38, 41, 42], scattering for thermography and mixing [43], and tracer-based measurements of mixing [44, 45]. With a trade-off in pulse energy, these systems are ultimately scalable to megahertz repetition rates [35, 41, 46]. The low duty cycle operation of these systems allows high pumping rates–achieving both high gain and high per-pulse energies ranging from 100's of mJ [36, 38, 39, 41] to >2 J [37, 43]. As continuously pulsed diode-pumped solid-state laser systems have also seen significant improvements in both repetition rate (10's of kHz) and pulse energy (10's of mJ/pulse) [47], it is now feasible to consider high-repetition rate, planar LII imaging with long record lengths using either burst-mode or continuously-pulsed laser systems.

In this work, the effects of repetitive pulsing on high-speed LII signals are investigated for long pulse-sequence durations and for a wider range of repetition rates and pump energies than what has been achieved in previous studies [17, 21, 31, 32]. A series of optical experiments is conducted in a laminar ethylene (C_2H_4) jet flame stabilized over a Santoro burner [48] to quantify LII signal degradation and recovery as a function of laser repetition rate and fluence during the course of a laser pulse sequence supplied by a burst-mode laser. These measurements are then extended to a pilot-stabilized turbulent jet flame to monitor the effects of repetitive laser heating under highly unsteady flow conditions. The LII signal evolution is evaluated for pulse-to-pulse temporal separations of 10-100 μs and for sequences of 100 to 1000 pulses while varying the laser fluence. In these measurements, the cumulative effects of multiple

probing on soot physical characteristics, local gas heating, and convective/diffusive replenishment of soot in the probe volume are potential sources of uncertainty. Planar images are also collected at rates of 10-50 kHz to investigate the ability to track soot layer thickness and soot structure evolution under various laser operating conditions. In this manner, the feasibility of achieving high-speed planar measurements of soot volume fraction is demonstrated, and experimental considerations to ensure accurate and repeatable results are considered.

2. Experimental apparatus

The burst-mode laser used in this work has been described in detail in previous publications [36, 38], and only a brief discussion of the system will be given here. The system, shown in Fig. 2(b), consists of a pulsed fiber oscillator (Manlight) which can operate from 100 kHz to 1 MHz, providing approximately 10 μJ/pulse. This pulse train is collimated and double-passed through a Gooch and Housego electro-optic modulator (EOM) for pulse selection and suppression of background amplified spontaneous emission (ASE) using the relatively short 200 ns EOM gate. This pulse selection is used to divide the initial oscillator frequency down to the desired repetition rate for planar LII measurements. Pulse sequences of 10-100 kHz are then passed through several amplifier chains consisting of both diode-pumped and flashlamp-pumped neodynium:yttria-aluminum-garnet (Nd:YAG) amplifiers. Depending on the selected repetition rate, the system can provide fundamental output at 1064 nm ranging from >200 mJ/pulse at 10 kHz to >15 mJ/pulse at 100 kHz. For the LII studies presented here, the fundamental output at 1064 nm was used with a burst duration of 10 ms.

In the current work, evaluation of the effects of repetitive pulsing on LII measurements only requires the use of the first four amplifiers (three diode-pumped and one flashlamp-pumped) to achieve fluences that can be used to evaluate the effects of repetitive pulsing. The near-Gaussian output ($M^2 < 1.5$) has negligible beam profile fluctuations over the burst, as previously reported [36]. For the majority of the experiments, the sheet was formed with a concave cylindrical lens and convex spherical lens to a height of 15 mm and focused to a full-width half maximum of ~350 μm measured using a scanning knife edge for the burst average. Typical operation for these experiments consisted of up to 3 mJ/pulse for a sheet of 7 mm height and up to 10 mJ/pulse for a 60 mm sheet height, resulting in fluences from 0.04 J/cm^2 to 0.5 J/cm^2. For planar LII imaging with larger fields of view or high repetition rates, it is possible to increase the burst-mode laser output energy and maintain similar fluences.

The multi-kHz LII signal from a single burst of laser pulses was collected by two separate techniques, as shown in Fig. 3. The first collection method consisted of a photomultiplier tube (Hamamatsu R1P28) with a bandpass filter from 425-465 nm and a typical time response of 2 ns. The PMT signal was sampled using an oscilloscope with a bandwidth of 1 GHz (Tektronix DPO7104). The PMT signal was collected via 1:1 imaging with a 75 mm lens and passed through an iris of 1 mm diameter placed immediately before the PMT and located in the imaging plane of the LII sheet. This resulted in an imaged area of 1 mm diameter in the center of the LII probe sheet. The 445 nm bandpass filter and PMT were located immediately behind this aperture. A photodiode trace from a single burst is represented in Fig. 2(a), where ~2 mJ/pulse at 50 kHz for a duration of nearly 10 ms was used to generate the the LII signal. The second collection system consisted of a dual-stage high-speed intensifier (Lavision, HS-IRO) equipped with a P43 phosphor, along with a lens-coupled high-speed CMOS camera (Photron SA-X2) and bandpass filter from 375-425 nm. The CMOS imaging system used a Nikon Nikkor f/2.8, 105 mm lens with a 20 mm extension tube to achieve higher magnification and a resultant field of view of 40 mm by 40 mm. For planar LII imaging, the HS-IRO used a 100 ns intensifier gate width with a 20 ns delay from the LII laser pulse. The 100 ns gate was the shortest possible using this intensifier, and the 20 ns delay was chosen to mitigate the effects of laser timing jitter and to avoid scattering of the probe at 1064 nm. The PMT measurement location was registered with the intensified image using a long exposure and residual scattering from a co-aligned helium-neon beam centered on the PMT aperture and imaged with the HS-IRO and CMOS high-speed imaging system.

The gray annular region in Fig. 3 depicts where the two burners used in this work were situated relative to the beam. For all studies, non-premixed ethylene was used. For laminar studies, a Santoro burner was utilized which consisted of an 11.11 mm (7/16") inner diameter brass fuel tube surrounded by a ceramic

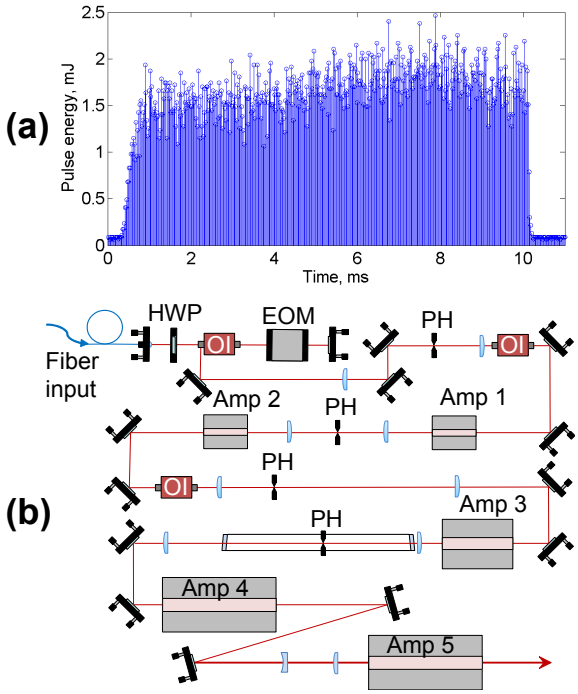

Fig. 2. Color available online. (a) Example laser pulse train at 50 kHz. (b) Burst-mode laser system consisting of a pulsed master oscillator which is fiber-coupled to a series of diode- and flashlamp-pumped amplifier stages. HWP, half-waveplate; EOM, electro-optic modulator; PH, pinhole; OI, optical isolator; Amp, amplifier.

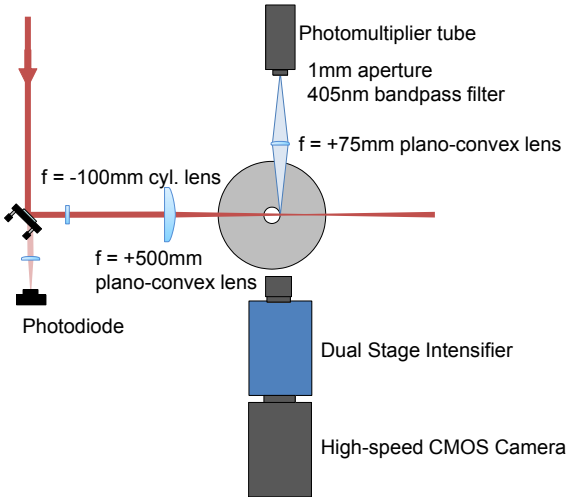

Fig. 3. Color available online. Diagram of system layout showing the burner placement (shaded region), LII probe beam, collimating sheet optics, a photodiode for energy normalization, a PMT with aperture, and coupled dual stage intensifier and CMOS camera for planar LII imaging.

matrix co-flow with both a diameter and height of 101.6 mm (4")[48]. The LII probe sheet was centered at a height of 30 mm above the burner exit, consistent with existing soot data taken on the burner [13, 48]. LII data with the PMT was collected in the annular, peak soot region where the peak soot volume fraction is $\sim 1 \times 10^{-5}$ [48]. For turbulent combustion studies, a piloted ethylene burner described by Zhang *et al.* [49] was utilized and included a pilot consisting of three rows of concentric holes around a $D = 3.2$ mm inner diameter fuel tube. The ethylene/air pilot was operated at an equivalence ratio of 1.0 and held at a fixed flowrate to match 2% of the total heat release of a Reynolds number $Re_D = UD/\nu = 20{,}000$ ethylene

jet flame. The pilot allowed jet-flame anchoring to a jet exit Reynolds number of Re_D = 25,000. The probe sheet was centered at a downstream position of 75 diameters, a location with large soot volume fraction for the relevant flow conditions [49].

3. Results and discussion

As previous studies discussed above have indicated, high-speed, multi-kHz LII measurements present some unique challenges because local heating of soot particles is required to achieve signal generation and can potentially be intrusive. Although laser-induced fluorescence measurements can also deposit significant amounts of energy through absorption, with careful selection of laser fluence and low gas tracer seeding densities, most multi-pulse effects can be avoided. A number of experiments in this work are focused on characterizing the degree of multi-pulse contamination and the intrusive effects of multiple subsequent probe pulses at different repetition rates and pulse energies. These effects are examined in both laminar and turbulent flame configurations.

3.A. Evolution of LII signal in laminar flame

To address the behavior of LII signals with multiple burst-mode probing, a series of measurements was collected in a laminar sooting flame stabilized on a standard Santoro burner. The laminar flame configuration with multiple probing is a worst-case scenario since the soot particles can remain in the same probe volume during much of the pulse burst. This repetitive interrogation of the same particles generates LII signal through repetitive heating or, in the case of high fluence LII probing, heating to the sublimation temperature.

The LII signal is measured with a photo-multiplier tube centered on the laser probe sheet and located at the annular, peak soot region of the Santoro flame. The 10 kHz LII signals over the duration of the pulse burst and for different probe fluences are shown in Fig. 4(a). Note that these plots do not represent LII transient signals in time resulting from a single pulse but rather shot-to-shot variations in LII signals collected from many laser shots during a 10 ms pulse burst. For consistency throughout the analysis, the LII signal is defined as the peak of the PMT signal recorded after each laser shot, unless otherwise noted. The general trends reported throughout the manuscript for variation over the bursts do not exhibit significant differences with signal gate durations varying from the peak signal to >5000 ns. For the lowest energy of 0.10 J/cm^2, there is no evidence of signal degradation over the 10 ms sequence of 100 pulses. A large degree of variation in the peak LII signal at low fluence is evident, as expected from the greater sensitivity of the LII signal to the laser fluence (as shown in Fig. 4(b)). As probe pulse fluence is increased, signal degradation becomes more apparent, but the decrease from the peak LII signal (early in the burst) is limited to <10% of signal amplitude for fluences up to 0.15 J/cm^2. A significant drop in the peak signal over the burst is evident for a higher pulse energy of 0.29 J/cm^2, which is within the typical LII signal plateau regime as shown in Fig. 4(a). This drop occurs rapidly, within <10 probe pulses, although the signal reaches a quasi steady-state value that is well below the maximum signal yield after about 20 pulses. These trends indicate that changes in the soot particle characteristics do not affect the LII signal substantially when the laser fluence is well below the signal plateau regime, even with long term repetitive pulsing. Since this regime is not typically associated with significant soot particle vaporization, this would indicate that the physical characteristics and transport properties of primary soot particles may not be altered significantly or have offsetting effects for low fluence pulse bursts.

Interestingly, all signals reach a steady state with repetitive pulsing, even for laser fluences in the high fluence regime. This steady state condition may arise from a reduced tendency of the soot particles to vaporize due to changes in chemical composition and mass loss, or because the rate of mass removal is in equilibrium with recondensation and replenishment via convection/diffusion after repetitive pulsing. Both the diffusive and convective timescales are estimated to be significantly longer than the interpulse time but may have an effect on the long-term signal after repetitive pulsing. For example, the LII probe location is centered on a LII probe sheet of 7 mm height, H. With the buoyancy-driven convective speed v measured

by Santoro *et al.* [50] of ∼1.4 m/s, the associated convective replenishment time to the probe volume is

$$\tau_{conv} = \frac{H/2}{v} = 2.5 \text{ ms}, \tag{1}$$

similar to the time to reach steady state in Fig. 4(a). An upper limit on the relevant timescale for replenishment of the probe volume through diffusion can be estimated simply based on bi-molecular diffusion of nitrogen in air as

$$\tau_d = \frac{\delta^2}{4D_g} \approx 0.5 \text{ ms}, \tag{2}$$

where the relevant length scale is the sheet thickness, δ =350 μm, and the diffusion coefficient, D_g, is taken as that of nitrogen in air at 1800 K. For diffusion of large (10's of nm) soot particles, this diffusivity will be orders of magnitude lower. Although typical thermophoretic velocities in regions of steep gradients may give similar timescales, for the replenishment of the probe volume with unperturbed soot, the azimuthal (out of plane) replenishment of the LII probe sheet would take place across a minimal temperature gradient. For moderate gradients of 100 K/mm, the thermophoretic velocities will be on the order of 1 cm/s [50], making the relevant timescale long as compared to the total laser interrogation time. As a result, estimates of convective and diffusive timescales imply that there is some influence of soot replenishment on LII signals during repetitive pulsing, but on a timescale that is longer than the interpulse spacing of 10 to 100 μs used in this study. As seen in the high fluence data in Fig. 4, a significant depletion occurs at early times and approaches steady state after a few milliseconds. This time to steady state is consistent with the time it takes soot to reach the PMT measurement location. After 2.5 ms, all soot reaching the measurement volume will undergo the same number of multiple probe pulses while being convected from the bottom of the laser sheet to the measurement location. Nevertheless, we must also consider the possibility that the approach to steady state may occur because of a balance between various other gain and loss mechanisms, such as gas expansion, gas heating, and out-of-plane convection/diffusion of fresh soot into the probe volume from outside the laser sheet, which will be examined further.

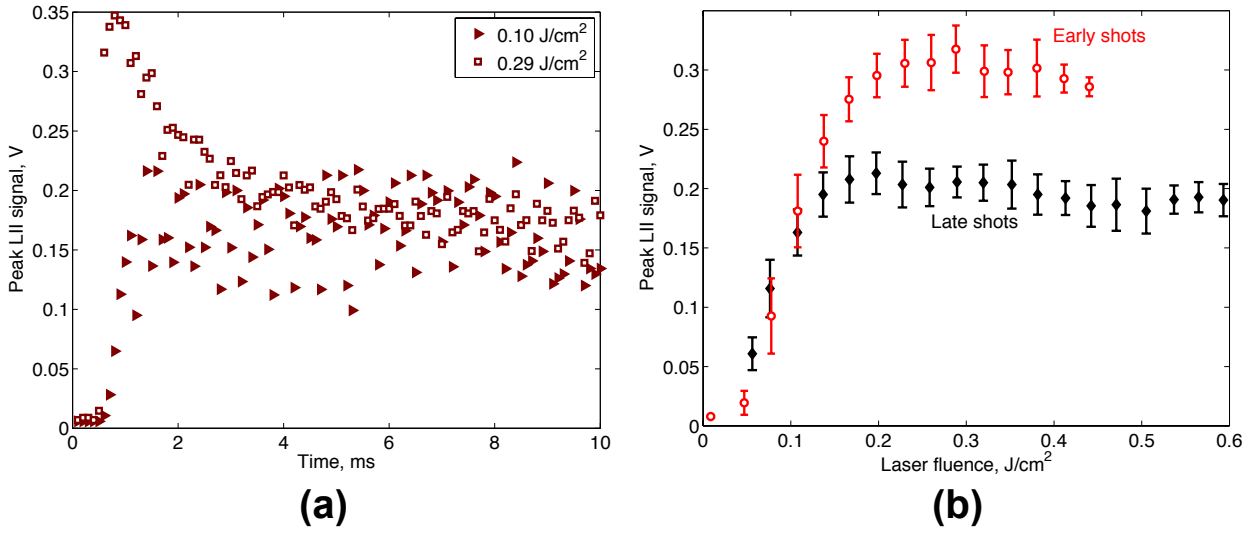

Fig. 4. Color available online. (a) 10 kHz, peak LII signal as a function of time during a 10 ms laser burst with varying pulse fluence and (b) peak LII signal as a function laser fluence early (<1 ms) and late (>9 ms) in the laser burst period. Error bars represent the standard deviation in peak signal for each laser fluence. Data were collected 30 mm above a laminar Santoro burner at the location of peak soot volume fraction.

In addition to examining the LII signal during the pulse sequence, it is of interest to evaluate the effects of laser fluence on the LII signal for pulses that are early in the laser burst period, when little signal

degradation is evident from the peak value in Fig. 4(a), compared to later in the burst period, when the signal reaches a lower steady state value. As shown in Fig. 4(b), for both early (<1 ms) and late (>9 ms) pulses in the burst, there is an initial rise in the LII signal with laser fluence, indicating increased heating of primary soot particles. The overlap in the LII signal levels at low laser fluences early and late in the burst also indicates minimal alteration of the soot physical characteristics by repetitive pulsing. At higher laser fluences, however, the trends in LII signal early and late in the burst begin to deviate, with signals from the early pulses reaching a plateau regime of LII signal that is about 50% higher than that of the signals from the later pulses. Note that the onset of the plateau regime occurring at a fluence of ~0.2 J/cm^2 seen for the early pulses in Fig. 4(b) is similar to that found in prior LII studies using traditional 10 Hz measurements with Gaussian laser sheet profiles [17, 26]. The slightly lower onset of the plateau for the later pulses indicates that the LII signal is more sensitive to changes in particle physical characteristics, which would be the case, for example, if the soot particle sizes were smaller later in the burst [16].

Another point of interest is in the individual pulse time response of the LII signal after repetitive laser heating. Two separate examples of the LII time response from different pulses in the burst are shown in Fig. 5. The upper panel shows the LII response for 5th and 95th pulses in a 100 pulse, 10 kHz burst at low fluence (0.11 J/cm^2). For these low fluence conditions, there is no evidence of a variation in the time decay of the LII signal when normalizing to the peak signal. A second case is shown in the lower panel of Fig. 5, where LII time decays are shown for the 5th and 95th pulses, but now at higher fluence (0.29 J/cm^2). At these conditions, well into the normal LII plateau regime, there is clear evidence of a faster time decay late in the burst. This change is indicative of faster particle cooling and is consistent with significant mass loss from primary particles due to repetitive heating.

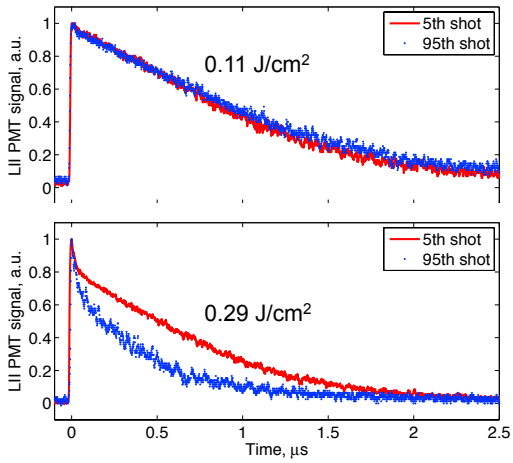

Fig. 5. Color available online. Time resolved LII signals normalized to the peak value. The upper panel shows the 5th and 95th LII signal in a 10 kHz, 100-pulse burst with an average fluence of 0.11 J/cm^2. The lower panel shows the same LII responses for the 5th and 95th pulses in a burst of 0.29 J/cm^2 average fluence.

For the case of a laminar flame with relatively slow rates of diffusion and convection as detailed previously, one would anticipate that the LII signal with repetitive pulsing would be sensitive primarily to interactions between the pump laser pulse and the soot primary particles. For the same per-pulse probe fluences, bursts at 10–100 kHz result in an order of magnitude difference in the average heating rate of the interrogated soot particles. Peak LII signals for repetition rates from 10–100 kHz are shown in Fig. 6(a) for identical average per-pulse laser energies that are below the threshold of the plateau regime for the case of 10 Hz probing (see Fig. 1(a)). From this comparison, it is clear that the average rate of energy absorption is an important parameter in the LII signal yield. This rate of energy absorption is more appropriately the cumulative effect of multiple LII probe pulses, each heating soot particles and resulting in significant absorbed energy. For this per-pulse fluence of 0.12 J/cm^2, no significant degradation is seen at 10 kHz and 20 kHz, while there is a ~30% degradation at 50 kHz, and ~70% at 100 kHz. This fluence is approximately equal to the threshold for limited vaporization loss determined by Witze *et al.* for 10 Hz measurements of

0.1 J/cm^2 [23], yet there is significant degradation of signal even at this relatively low fluence for >20 kHz probing. At high fluences this effect becomes more pronounced, as evident in the bursts shown in Fig. 6(b) for a repetition rate of 50 kHz. As the repetition rate, or average heating rate over the burst, increases, the significant drop in LII signal yield occurs over shorter and shorter timescales. It is important to note, however, that even at high repetition rates, the LII signal seems to come to a steady state after many pulses. For all the cases shown in Fig. 6(a), the steady state seems to occur at a similar point in time–near the estimated time of 2.5 ms for soot to convect from the bottom edge of the probe sheet to the PMT measurement location (when all the soot entering the probe volume will have the same time history). At a high fluence of 0.26 J/cm^2 and repetition rate of 50 kHz, however, the decay in the LII signal shown by the solid line in Fig. 6(b) should be fast enough to completely deplete the signal prior to 2.5 ms. Note that the solid lines were obtained by assuming fractional per-pulse depletions of ℓ_p =0.0004, 0.006, and 0.012 from low to high fluence, respectively. Even for faster decay rates at 100 kHz (not shown), the signal reaches a steady state prior to 2.5 ms rather than approaching zero. The discrepancy can be explained by fresh soot exchange through either diffusion or out-of-plane convection. This suggests that a balance is achieved between the various loss and gain processes in the probe volume, where laser-induced changes in soot characteristics are offset by effects such as replenishment of fluid and local gas heating within the probe volume. If there are other signal gain mechanisms leading to a non-zero steady state at high fluence, then it is possible that the LII signal losses due to changes in soot physical properties may be higher than expected and are continuously being offset by other gain mechanisms such as replenishment of soot via out of plane convection/diffusion of fresh soot.

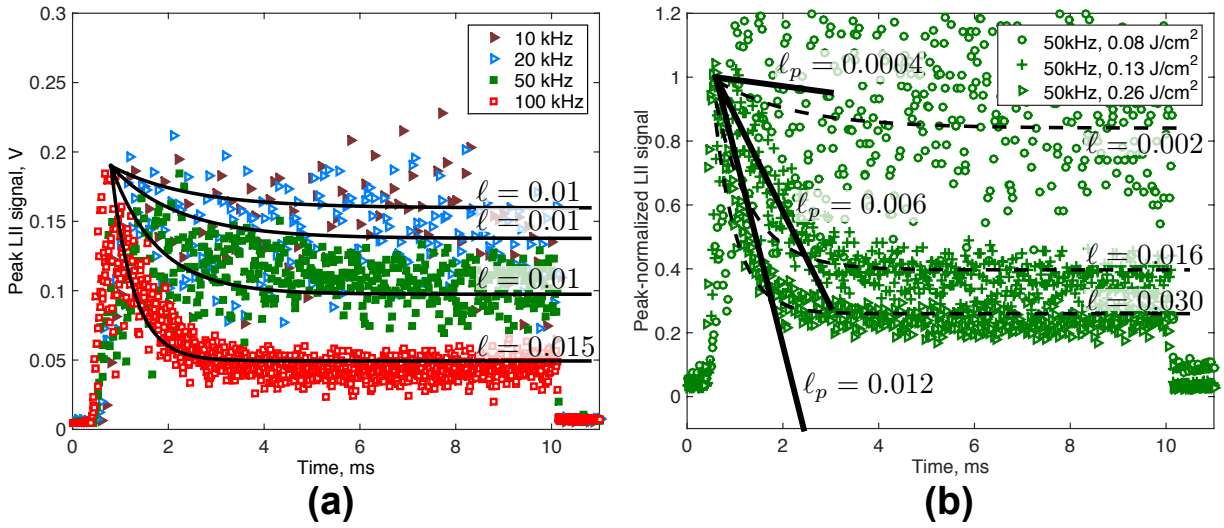

Fig. 6. Color available online. (a) Variation of the peak LII signal of individual pulses for burst repetition rates of 10–100 kHz at a fixed laser fluence of 0.12 J/cm^2. Solid lines show various loss rates ℓ with the gain rates corresponding to repetition of g =0.05, 0.025, 0.01, and 0.005. (b) High fluence, peak LII signals for repetition rates of 10–100 kHz showing strong signal decrease over the early part of the burst duration. Solid lines indicate linear signal decay associated with constant per-pulse loss for one convective timescale and dashed lines indicate cumulative loss, bounding the possible range of loss rates.

To obtain an upper limit on the possible loss rates, consider instead a fractional loss ℓ due to repetitive laser pulsing and a fractional exchange of gas g in the probe volume based upon the convective and diffusive timescales previously discussed. The gain estimate here assumes fresh (out-of-plane) soot entering the measurement volume at the estimated convective speed rather than soot that has been probed multiple times as it travels from the bottom of the laser sheet to the PMT measurement location. Nevertheless, this simple analysis can put an upper limit on the loss rate by defining an expression for the LII signal after the nth probe,

$$C_n = C_{n-1}(1-\ell)(1-g) + C_0 g, \tag{3}$$

which can be written based on the signal after the $n-1$ probe, C_{n-1}, and a convective/diffusive exchange of g with the unperturbed concentration C_0. With every laser probe, there is some short time to have some exchange with fresh soot, and the signal of the nth pulse can then be written as

$$C_n = C_0\left((1-\ell)^n(1-g)^n + \sum_{p=0}^{n} g(1-\ell)^p(1-g)^p\right). \tag{4}$$

Examining this expression, an asymptote can be determined for fractional values of ℓ and g, given by

$$C_\infty = C_0\frac{g}{g+\ell-g\ell}. \tag{5}$$

The magnitude of loss and gain from Eq. 5 can be used to estimate the progressive effects of repetitive laser heating on the LII signal. Four representative curves using Eq. 5 are compared with the experimental data in Fig. 6(a). To be consistent with the convective/diffusive time scales noted earlier, fractional gains due to refilling are estimated at $g = 0.05$, 0.025, 0.010, and 0.005 per pulse for repetition rates of 10, 20, 50 and 100 kHz, respectively. As the nominal per-pulse laser energy is the same in each of the four repetition rates, the loss rate due to repetitive laser pulsing should also be the same. Indeed, loss rates of $\ell = 0.01$ per pulse result in a good match to the experimental trends from 10–50 kHz, while a loss rate of $\ell = 0.015$ is needed to match the experimental data at 100 kHz. The predicted curves using these simple assumptions track the variation in the LII signal intensity as well as the rate of signal decay over the duration of the pulse burst for the widely varying repetition rates in Fig. 6(a). Of course, this analysis does not distinguish between different possible mechanisms that may result in the net loss from repetitive laser pulsing (e.g., vaporization, local gas heating, recondensation), and the actual loss rate is only an estimate based on gas exchange timescales. However, based on results from these laminar flame studies where the gas exchange process is relatively constant, it may be possible to treat the net effect of various loss mechanisms consistently from shot to shot. Hence, the rate of signal loss as a function of time may be a predictable function of the laser fluence and repetition rate.

More importantly, these pulse-to-pulse loss rates estimated by ℓ represent an upper bound assuming that this loss is being offset by fresh soot being brought into the probe volume from out of the plane of the laser sheet at the full axial convective velocity. If the actual case is one in which soot is convecting into the probe volume primarily from axial convection within the plane of the laser sheet, then the actual loss rate may be closer to ℓ_p. For example, in the case of 50 kHz and 0.08 J/cm^2, as shown in Fig. 6(b), the pulse-to-pulse fractional signal loss is bounded at the low end by $\ell_p \approx 0.0004$ and at the high end by $\ell = 0.002$ using Eq. 4. Hence, by reducing the laser fluence, a regime with a relatively low net loss rate (<1%) can be achieved on a pulse-to-pulse basis, which is consistent with the results of Fig. 5(a). In turbulent flames where gas exchange processes dominate, it should be possible to ignore such a per-pulse loss rate as it is unlikely that the same soot particle will remain in the 350 μm wide probe volume for many consecutive pulses. It should be feasible, therefore, to relate the LII signal to the locally varying soot volume fraction and ignore the effects of repetitive laser heating at low fluence. Even at high fluence in Fig. 6(b), the lower and upper bounds on the pulse-to-pulse fractional signal loss are $\ell_p = 0.012$ and $\ell = 0.03$, respectively, which may not significantly impact the soot volume fraction measurements if turbulent time scales that are no more than a factor of two or three longer than the pulse-to-pulse temporal separation. Of course, the precise gain and loss mechanisms for the LII signal are not known and are of interest in future work, as there may be multiple offsetting effects from the laser-soot particle interaction, including changes in soot physical characteristics, local gas heating, and changes in transport processes.

With clear evidence of fluence dependent signal degradation over the burst duration even with laser fluences that are low relative to 10 Hz LII experiments (0.1 J/cm^2), a more detailed investigation of the LII signal versus laser fluence was undertaken at various fixed repetition rates. A subset of this data is presented in the plots of peak LII signal versus per pulse laser fluence in Fig. 7. For repetition rates from 10–100 kHz, there are narrow ranges in which the signal dependence is nearly linear with laser fluence, as shown in Fig. 7(a). As the repetition rate is increased (i.e., at higher average irradiance), the peak LII signal shifts to lower fluence. The data in Fig. 7(a) correspond to the regime before the LII signal versus laser fluence reaches a plateau, so it is interesting to note the average irradiance for each repetition rate

and per-pulse fluence, F. For these cases, the average irradiance,

$$I_{avg} = \frac{F \times N_p}{\tau_{burst}}, \tag{6}$$

ranges from 1400 to 7000 W/cm^2, where N_p is the number of pulses and τ_{burst} is the length of the burst. At higher per-pulse fluences, large differences in signal yield with fluence are shown in plotting per pulse LII signal versus laser fluence in Fig. 7(b). Here the maximum average irradiance varied from 6000 to 45000 W/cm^2. As the repetition rate increases (higher average irradiance), the cumulative effect of multiple LII probing results in a shift in the peak of the LII signal yield to lower fluence and a decrease in the maximum and high fluence LII intensities. A rescaling of the both the low and high fluence data shown in Figs. 7(a) and 7(b) using the average irradiance does not contribute to a meaningful interpretation of this data, as the effects are those of cumulative energy absorption.

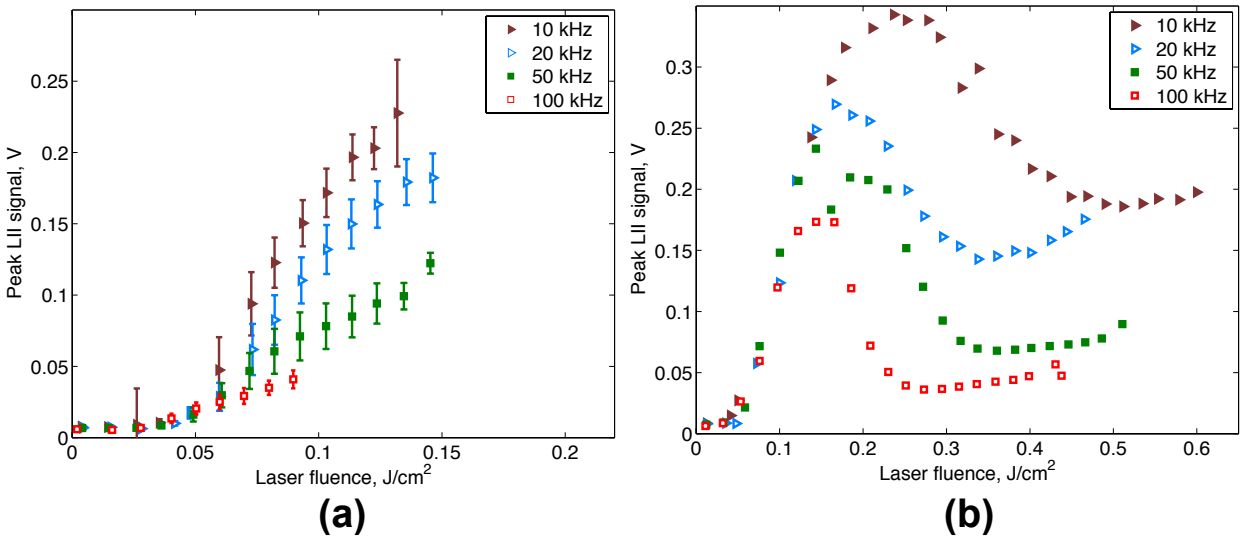

Fig. 7. Color available online. Fluence dependence of peak LII signal registered with a PMT for multiple burst repetition rates in (a) a low fluence regime, and (b) a high fluence regime. Error bars indicate variance in shot-to-shot signal. Peak LII signals and laser fluences are included over the duration of the 10 ms bursts.

As noted earlier in Fig. 7(a), there are regions of nearly linear dependence with fluence at <0.1 J/cm^2. For repetition rates of 10, 20, 50, and 100 kHz and for fluences of <0.1 J/cm^2, a linear fit, $S_{norm}(F) = mF+b$, is identified and a linear least squares fit slope m and intercept b are determined for each repetition rate. This fluence-dependent function can be used to normalize the data in the low fluence regime. The peak LII signals of Fig. 8(a) are normalized based on these calibrated fits, and the normalized signals are shown in Fig. 8(b) for repetition rates of 10–100 kHz. These normalized curves show little variation over the burst duration, while the scatter is due to the strong sensitivity of the peak LII signal to laser fluence. This study indicates that a quasi-linear signal dependence is evident for repetition rates up to 100 kHz, and a calibrated normalization is possible.

The constant signal yield over the burst in Fig. 8 also indicates that the net loss in LII signal due to repetitive probe effects can be minimized even at high repetition rates by reducing the laser fluence. Compared with the data in Fig. 6(a), in which LII signals were generated with a constant fluence of 0.12 J/cm^2 for all repetition rates, the data in Fig. 8 were acquired using lower fluences of 0.10 J/cm^2 at 10 kHz and 20 kHz, 0.08 J/cm^2 at 50 kHz, and 0.04 J/cm^2 at 100 kHz. At the lower fluences, the data for repetition rates from 10–100 kHz showed no appreciable deviation from the steady state behavior. This is in agreement with the data of Fig. 5(a), which show that the soot particle cooling rate associated with particle mass and/or size does not change appreciably from early to late in the burst for the case of low fluence. Of course, there are other mechanisms that may also be important in contributing to the net loss in LII signal during repetitive pulsing, such as soot recondensation or local gas heating [33, 34]. The data

in Fig. 8 imply that either (1) the effects of these mechanisms are minimized at low fluence or (2) multiple mechanisms are very precisely offsetting each other to give an overall negligible effect during repetitive pulsing over a wide range of conditions. In either scenario, it is reasonable to conclude that the low fluence condition minimizes the impact of repetitive pulsing, allowing the LII signal to be related to local soot volume fraction during the pulse burst. This gives practical guidance for the laser fluences that can be used for soot volume fraction measurements over a wide range of flow rates, even under conditions when soot in in the probe volume may be probed multiple times.

While these results are encouraging for burst-mode LII measurements in laminar and turbulent flames, it is also of fundamental interest to take into account the current data and consider whether it is possible to discern the contribution of different mechanisms to the net zero change in LII signal during a pulse burst at low fluence. In this regard, the macroscale trends in the current data do not provide strong evidence that multiple laser-soot interaction mechanisms (vaporization, gas heating, recondensation) are offsetting each other and leading to a zero net change in LII signal. First, there is no evidence of soot particle mass loss or size changes in the low fluence regime, as shown in Fig. 5(a). Second, the LII signal during repetitive pulsing is quite sensitive to the pulse-to-pulse loss rate, so multiple mechanisms that affect the LII signal would have to perfectly offset each other to within 1% to avoid significant changes in the time history of the LII signal. Moreover, if these mechanisms are offsetting each other to less than 1%, this is taking place even while changing the fluence at a constant repetition rate and vice versa. Considering the evidence, it seems more likely that a low fluence regime exists in which all of the possible mechanisms leading to LII signal losses are negligible relative to the rate of convective/diffusive soot replenishment.

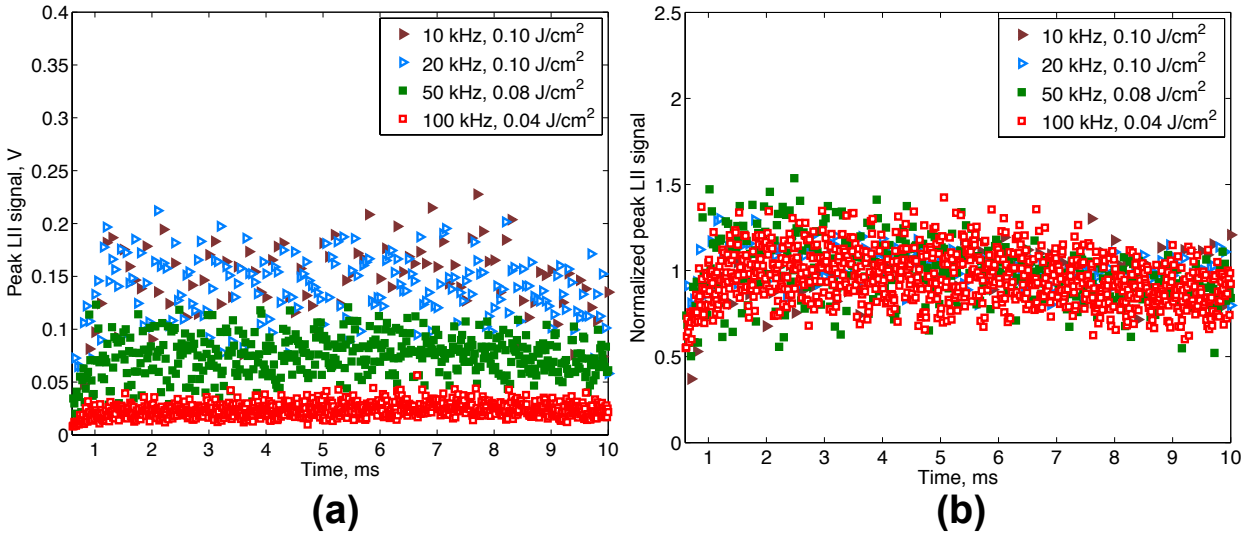

Fig. 8. Color available online. Low fluence peak LII response for repetition rates of 10 kHz, 20 kHz, 50 kHz, and 100 kHz with (a) raw peak signal and (b) normalization using a linear fit to the repetition rate dependent low fluence responses shown in Fig. 7(a).

For relevant high-speed soot-layer imaging, there are two potential goals which may be achieved independently. First, there is an interest in making absolute soot volume fraction measurements. Even a relative measurement of soot volume fraction requires a clear dependence of signal on the probe fluence. Based on the effects observed at high repetition rate, the LII plateau regime is not an option and fluences must be limited to a fairly narrow range where predictable, monotonic signal dependence is evident. Second, there is interest in the tracking of soot structures. In this case, a quantitative soot volume fraction measurement is not essential so long as structures can be tracked with high fidelity. In order to assess the ability to track features, high repetition rate LII imaging was performed in a laminar ethylene non-premixed flame on a Santoro burner. The first criterion for soot structure tracking is a sufficient signal to noise ratio (SNR) in order to differentiate between regions of low and high soot volume fraction. Here, the SNR is defined as the ratio of the mean signal near the maximum soot volume fraction to the standard deviation of the LII background image, where both are taken across a 10 pixel by 10 pixel area. For the low fluence

cases in the laminar Santoro flame presented in Fig. 8(a), the typical signal to noise ratios range from 140 (at 10 kHz, 0.12 J/cm^2) to 30 (at 100 kHz, 0.045 J/cm^2). To assess the influence of multiple probe pulses on the measured soot layer thickness in this laminar flame, the width of the soot layer was tracked as a function of the time and the probe pulse number for repetition rates from 10 to 100 kHz. The full width half-maximum (FWHM) of the soot layer in this laminar flame is shown in Fig. 9(a) for multiple repetition rates at low fluences (< 0.1 J/cm^2). The FWHM was determined from a 40 pixel vertical bin of the LII images centered at a height of 30 mm above the tube exit. For fluences below the onset of the plateau observed in the LII fluence dependence, there are no significant effects during the burst duration. For high LII fluences, effects can be seen in the laminar flame for higher repetition rates of 50 and 100 kHz, as shown in Fig. 9(b). Although it will not be addressed in detail here, some of this effect arises from the change of the structure of the flame with repeated probing and is likely due to repeated energy absorbed in the LII probing as well as resultant gas heating and thermal expansion. Nevertheless, at rates less than 50 kHz, it is clear that tracking soot features is feasible with small influence of the repeated probing in laminar flames.

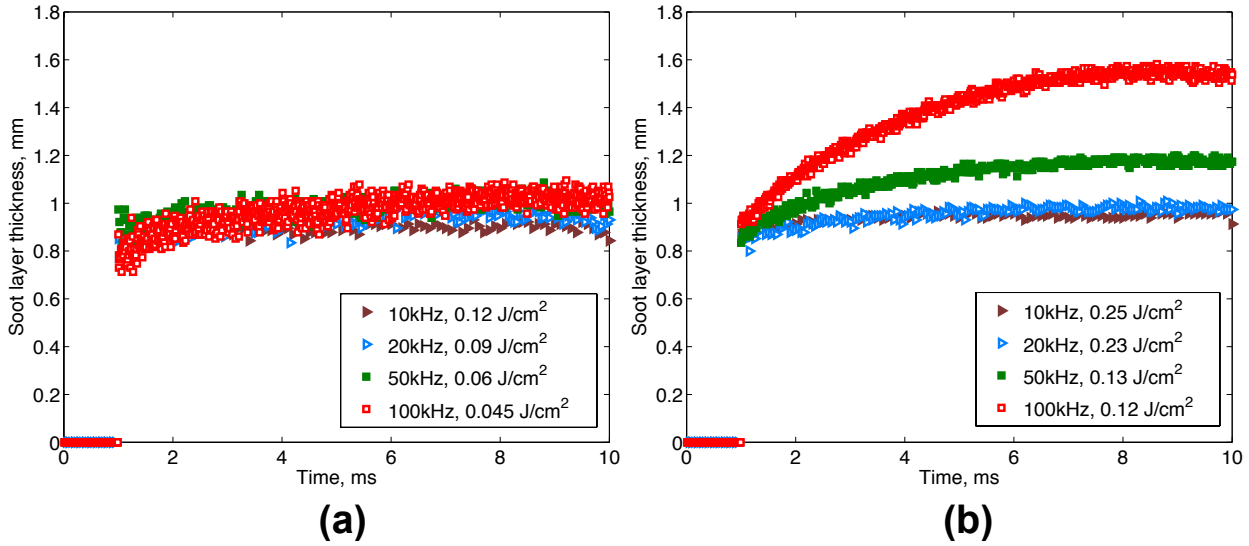

Fig. 9. Color available online. Variation in measured soot layer FWHM from high-speed LII imaging at 50 kHz during a 10 ms burst for (a) the low fluence and (b) high fluence regimes.

3.B. Burst-mode LII in turbulent flames

To assure the reliability and consistency of multi-kHz soot imaging, the turbulent burner described previously was used to evaluate both point and planar LII signals as a function of laser fluence and repetition rate. As determined by the laminar flame studies above, there is a clear difference in the LII signals in time between a low and high fluence regime. In the case of turbulent flames, the majority of the measurements detailed here are taken at a downstream distance of $z/D = 75$, near the peak of maximum soot volume fraction [49]. The time-averaged LII signal over 100 bursts for each of the 100 pulses in a 10 kHz train is shown in Fig. 10(a) versus the laser fluence. As expected from the laminar flame results at low fluence, a predictable, monotonic relationship between LII signal and laser fluence is evident in this low fluence regime. The pulse-fluence normalized and time-integrated LII signals over the burst are shown for Reynolds numbers of $Re_D = 10{,}000$ and 20,000 for both a low fluence and high fluence regime in Fig. 10(b). Here a pulse-fluence normalization was applied simply to show the rapid drop off in signal in the high fluence cases. For both low fluence cases, the normalized LII signal remains relatively constant over the pulse number. For both high fluence cases, there is a rapid decline in signal within the first $\sim$5 pulses.

Two sample image sequences are shown at 10 kHz and 50 kHz repetition rate in Figs. 11 and 12,

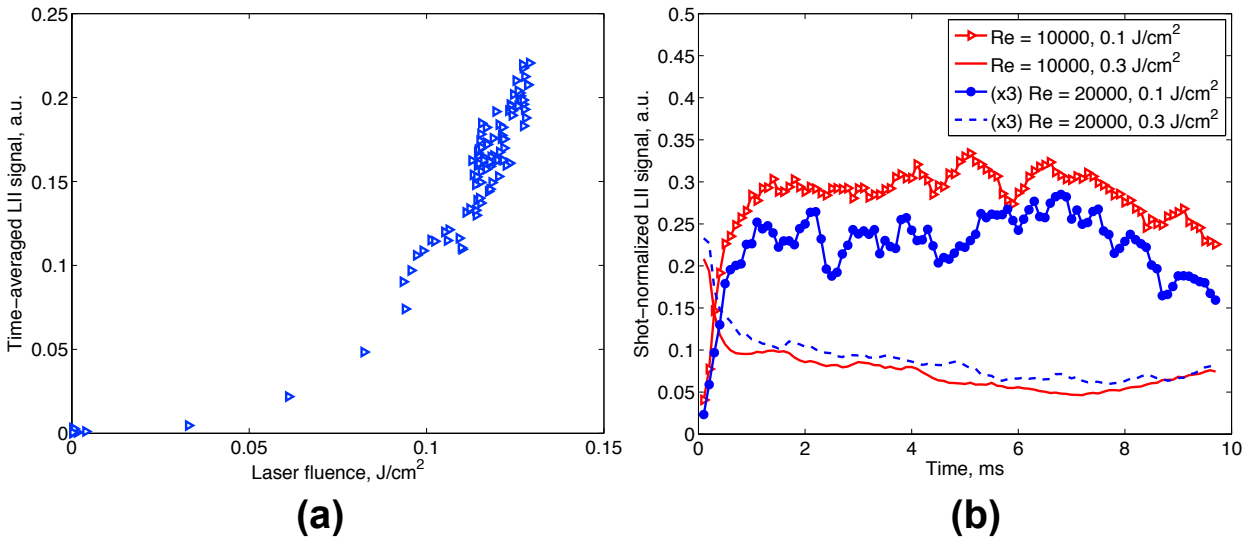

Fig. 10. Color available online. (a) Time-averaged LII signal dependence on averaged laser fluence for 10 kHz bursts averaged over 100 bursts in the $Re_D = 20{,}000$ turbulent jet flame at $z/D = 75$. (b) Variation of LII signal with the laser fluence over a 100-burst average in the Sandia $Re_D = 10{,}000$ piloted ethylene flame at $z/D = 75$. Curves with markers show the low fluence regime (0.1 J/cm^2) and lines indicate the high fluence regime (0.3 J/cm^2).

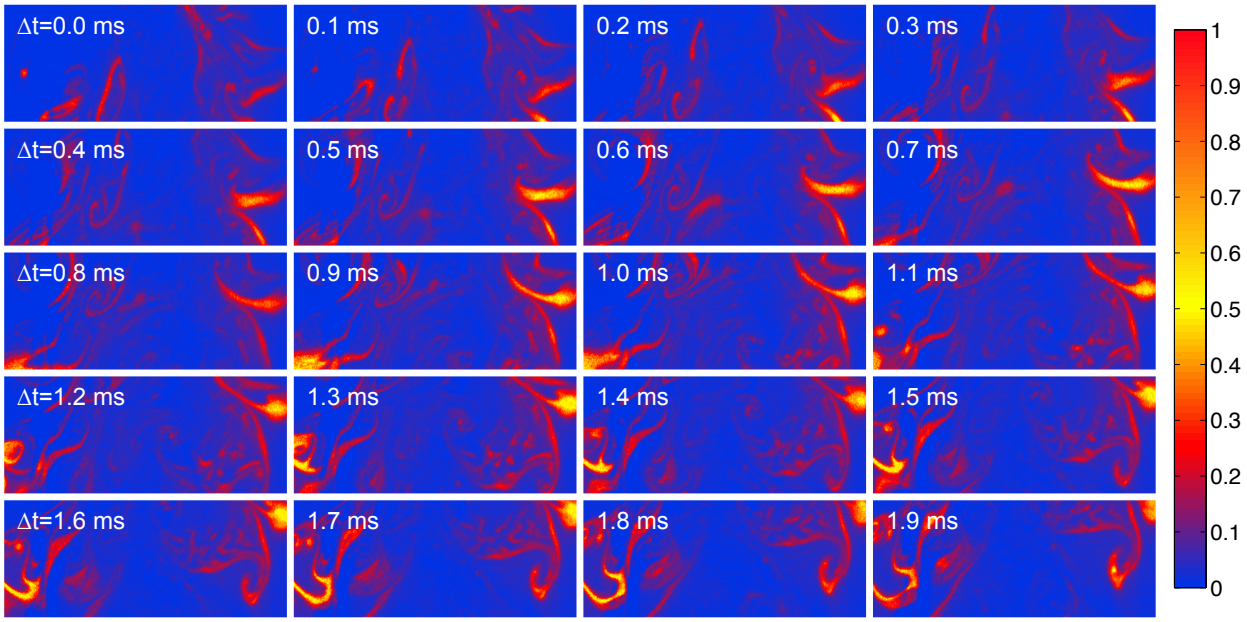

Fig. 11. Color available online. Sample LII image series at a 10 kHz repetition rate in the low fluence regime previously identified (0.11 J/cm^2). Images are taken centered at an axial location of z/D of 75 and centered over the jet in a $Re_D = 20{,}000$ non-premixed, piloted ethylene flame.

respectively. These series are centered at z/D of 75 in the shear layer of the turbulent non-premixed jet flame with a jet exit Reynolds number of $Re_D = 20{,}000$. The 10 kHz series in Fig. 11 is taken in the low fluence regime (0.11 J/cm^2), with every frame shown. The 50 kHz series in Fig. 12 is taken in the high fluence regime (0.29 J/cm^2), with every 5th image shown for comparison to the 10 kHz series. Images show a dark subtracted and peak-signal normalized map. In both the low and high fluence regimes, fine structures are evident and good frame-to-frame correlation seems to be evident in both sets. For these image series, in regions of maximum LII signal, typical signal-to-noise ratio ranges from 80 for the 10 kHz,

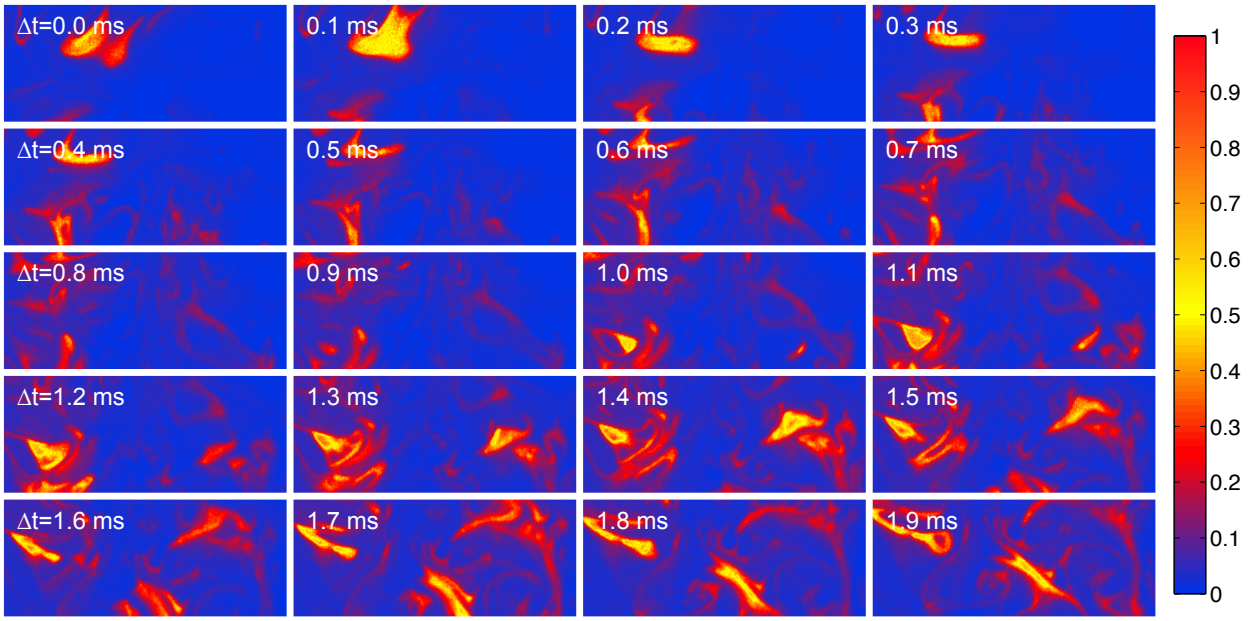

Fig. 12. Color available online. Sample LII image series at a 50 kHz repetition rate in the high fluence regime previously identified (0.29 J/cm^2) with every 5th image shown. Images are taken centered at an axial location of z/D of 75 and centered over the jet in a Re_D = 20,000 non-premixed, piloted ethylene flame.

low fluence case to 120 for the 50 kHz, high fluence case.

As discussed earlier, the study of turbulent sooting flames often requires only a qualitative imaging of soot structures. For example, the production of soot structures in the midst of a turbulent three-dimensional flow field and a reaction front requires the ability to track a particular soot structure with good fidelity. This does not necessitate a direct knowledge of the absolute or relative soot volume fraction so long as structures can be tracked. Although the image series of Figs. 11–12 show good correspondence of structures between individual frames, a detailed knowledge of the correlation between structures in a time-resolved set of images is useful in detailing the ability to track particular soot structures. With this in mind, the autocorrelations between multiple images of several 50 kHz image series were examined. The goal of the autocorrelation calculation is to elucidate differences between a low fluence and high fluence regime and verify similar autocorrelation behaviors in time.

The autocorrelation R_i is defined by a 10 by 10 pixel binning around a single point,

$$R_i(\tau) = \int_N^N S_i(t) S_i(t+\tau), \tag{7}$$

with the signal at a location i and time t defined as $S_i(t)$. The autocorrelation was calculated at two different points indicated in Fig. 13 for two 50 kHz image series to look for any differences with increased fluences. If significant signal degradation leading to a decrease in LII structure size were taking place, this should manifest in a shorter time to de-correlation. The autocorrelations were calculated at two points (A and B), indicated in Fig. 13(a) for fluences of 0.09 J/cm^2 and 0.15 J/cm^2 for 10 laser bursts. The average convective time through the LII probe volume at the sample location is ∼1 ms, so the autocorrelation is performed over ∼100 soot structures. The result of this autocorrelation is shown in Fig. 13(b). For these two points and two fluences, there is little change in the autocorrelation structure. Over 10–15 time intervals between pulses (200–300 μs) the autocorrelations show negligible difference. At longer time, there are small differences in the two autocorrelations at the high fluence condition. From the image series presented and this calculated autocorrelation for these two fluences, there is good evidence that structures can be tracked with good fidelity, even at high laser fluences.

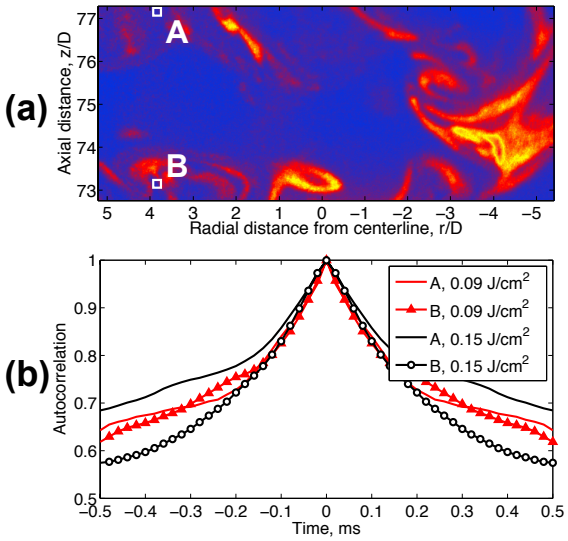

Fig. 13. Color available online. (a) Two points, A and B for which autocorrelations are calculated over 10 laser bursts. (b) Autocorrelation for fluences of 0.09 J/cm^2 and 0.15 J/cm^2.

4. Conclusions and guidelines for high-speed LII imaging

Laser-induced incandescence (LII) signals during repetitive laser probing in non-premixed sooting flames were evaluated under laminar and turbulent conditions for the fundamental 1064 nm output of an Nd:YAG burst-mode laser. Laminar flames were used to investigate the effects of laser fluence and repetitive pulsing on the LII signal over sequences of up to 1000 pulses. Turbulent flames were used to evaluate the laser fluence that would be sufficient for achieving the signal-to-noise ratio and spatial resolution needed to image fine soot structures at rates up to 100 kHz.

Laminar flame studies of burst-mode LII signals showed the existence of a low fluence regime in which the LII signal remained constant in time during the burst sequence. The departure from the low fluence regime depends on the cumulative effects of multiple laser probe pulses, not just the peak fluence during an individual pulse. Laser fluences of about 0.10 J/cm^2 ensured constant LII signals for repetition rates of 10–20 kHz, while laser fluences of 0.08 J/cm^2 and 0.04 J/cm^2 enabled constant LII signals at 50 and 100 kHz, respectively. The latter two fluences are below the 0.1 J/cm^2 cutoff that has been reported as the vaporization onset limit in prior 10 Hz LII studies [23], indicating that even small amounts of mass loss can affect the long-term signal under repetitive pulsing, especially at high repetition rates. Simple models of cumulative LII signal losses versus soot replenishment through convection/diffusion confirmed that constant LII signals could be attained with low fluence in laminar flame studies with estimated net loss rates of $<1\%$ per pulse. At higher fluence, significant LII signal degradation occurred in laminar flames, implying substantial changes in soot characteristics were occurring. Nonetheless, the low fluence regime produced sufficient LII signals to allow relative measurements of soot volume fraction at rates up to 50 kHz.

The low LII signal losses for the low fluence regime in laminar flames imply that it should also be possible to relate the LII signal to the local soot volume fraction in turbulent flames because of the much shorter convective/diffusive time scales. The low fluence regime allowed sufficient signal-to-noise ratio and spatial resolution for imaging fine soot structures at rates up to 50 kHz. At higher repetition rates, the laser energy necessary to produce sufficient LII signals was beyond the low fluence regime identified in the laminar flame studies. Nonetheless, for many applications, the identification of particular soot structures may be of interest in examining interactions between local chemistry and the three-dimensional velocity field during soot precursor formation and intermittent, localized soot formation/oxidation. It was shown that even for fluences found to be strongly altering and potentially intrusive at repetition rates up to 100 kHz, it is possible to track soot structures of interest with good fidelity. Soot layers in laminar

flames maintained approximately constant thickness even with high repetition rates. In turbulent flames, an examination of the cross-correlation between images showed little difference between low and high fluences, indicating that structure tracking is feasible.

In summary, we demonstrated a large increase in the repetition rate for planar soot LII imaging up to 100 kHz. This increase in repetition rate allows probing of fluid-flame interactions at much greater turbulent Reynolds numbers than previous studies. In demonstrating this capability, the intrusive nature of multiple probing was investigated, with the identification of a simple model to estimate bounds for the LII signal loss at low fluence and high fluence regimes. This measurement capability and the identification of these regimes provide a guide for future soot imaging studies and indicates the potential for quantitative, time-resolved studies of soot formation and oxidation during fluid-flame interactions.

Acknowledgments

Funding was provided by the Air Force Office of Scientific Research (Dr. Chiping Li, Program Manager). Support for CRS was provided by Sandia's Laboratory Directed Research and Development (LDRD) program. Sandia National Laboratories is a multiprogram laboratory managed and operated by Sandia Corporation, a wholly owned subsidiary of Lockheed Martin Corporation for U.S. DOE's National Nuclear Security Administration under contract DE-AC04-94AL85000.

References

[1] I. Glassman and R. Yetter, *Combustion* (Academic Press, 2008).
[2] J. O'Connor and M. Musculus, "Post injections for soot reduction in diesel engines: A review of current understanding," SAE Technical Paper 2013-01-0917, SAE International, Warrendale, PA (2013).
[3] S. Curran, R. Hanson, R. Wagner, and R. D. Reitz, "Efficiency and emissions mapping of RCCI in a light-duty diesel engine," SAE Technical Paper 2013-01-0289, SAE International, Warrendale, PA (2013).
[4] M. P. B. Musculus, P. C. Miles, and L. M. Pickett, "Conceptual models for partially premixed low-temperature diesel combustion," Progress in Energy and Combustion Science **39**, 246–283 (2013).
[5] T. V. Johnson, "Review of diesel emissions and control," International Journal of Engine Research **10**, 275–285 (2009).
[6] T. C. Lieuwen and V. Yang, *Gas Turbine Emissions*, vol. 38 (Cambridge University Press, 2013).
[7] H. Wang, "Formation of nascent soot and other condensed-phase materials in flames," Proceedings of the Combustion Institute **33**, 41–67 (2011).
[8] F. Bisetti, G. Blanquart, M. E. Mueller, and H. Pitsch, "On the formation and early evolution of soot in turbulent nonpremixed flames," Combustion and Flame **159**, 317–335 (2012).
[9] M. E. Mueller and H. Pitsch, "LES model for sooting turbulent nonpremixed flames," Combustion and Flame **159**, 2166–2180 (2012).
[10] C. R. Shaddix, J. E. Harrington, and K. C. Smyth, "Quantitative Measurements of Enhanced Soot Production in a Flickering Methane/Air Diffusion Flame," Combustion and Flame **99** 723–732 (1994).
[11] D. O. Lignell, J. H. Chen, P. J. Smith, T. Lu, and C. K. Law, "The effect of flame structure on soot formation and transport in turbulent nonpremixed flames using direct numerical simulation," Combustion and Flame **151** 2–38 (2007).
[12] R. J. Santoro and C. R. Shaddix,"Laser-Induced Incandescence," in *Applied Combustion Diagnostics,* K. Kohse-Höinghaus and J.B. Jeffries, eds. (Taylor and Francis, New York, 2002) pp. 252-286.
[13] B. Quay, T. W. Lee, T. Ni, and R. J. Santoro, "Spatially resolved measurements of soot volume fraction using laser-induced incandescence," Combustion and Flame **97**, 384–392 (1994).
[14] B. Axelsson, R. Collin, and P.-E. Bengtsson, "Laser-induced incandescence for soot particle size measurements in premixed flat flames," Applied Optics **39**, 3683–3690 (2000).
[15] M. F. Modest, *Radiative heat transfer* (Academic Press, 2013).
[16] H. A. Michelsen, F. Liu, B. F. Kock, H. Bladh, A. Boiarciuc, M. Charwath, T. Dreier, R. Hadef, M. Hofmann, J. Reimann, S. Will, P.-E. Bengtsson, H. Bockhorn, F. Foucher, K.-P. Geigle, C. Mounaïm-Rousselle, C. Schulz, R. Stirn, B. Tribalet, and R. Suntz, "Modeling laser-induced incandescence of soot: a summary and comparison of LII models," Applied Physics B **87**, 503–521 (2007).

[17] K. A. Thomson, K. P. Geigle, M. Köhler, G. J. Smallwood, and D. R. Snelling, "Optical properties of pulsed laser heated soot," Applied Physics B **104**, 307–319 (2011).
[18] H. Bladh and P.-E. Bengtsson, "Characteristics of laser-induced incandescence from soot in studies of a time-dependent heat- and mass-transfer model," Applied Physics B **78**, 241–248 (2004).
[19] C. Schulz, B. F. Kock, M. Hofmann, H. Michelsen, S. Will, B. Bougie, R. Suntz, and G. Smallwood, "Laser-induced incandescence: recent trends and current questions," Applied Physics B **83**, 333–354 (2006).
[20] M. K. Bobba and M. P. B. Musculus, "Laser diagnostics of soot precursors in a heavy-duty diesel engine at low-temperature combustion conditions," Combustion and Flame **159**, 832–843 (2012).
[21] R. L. Vander Wal and K. A. Jensen, "Laser-induced incandescence: excitation intensity," Applied Optics **37**, 1607–1616 (1998).
[22] R. L. Vander Wal and M. Y. Choi, "Pulsed laser heating of soot: morphological changes," Carbon **37**, 231–239 (1999).
[23] P. O. Witze, S. Hochgreb, D. Kayes, H. A. Michelsen, and C. R. Shaddix, "Time-resolved laser-induced incandescence and laser elastic-scattering measurements in a propane diffusion flame," Applied Optics **40**, 2443–2452 (2001).
[24] R. L. Vander Wal, T. M. Ticich, and A. B. Stephens, "Optical and microscopy investigations of soot structure alterations by laser-induced incandescence," Applied Physics B **67**, 115–123 (1998).
[25] N. H. Qamar, Z. T. Alwahabi, Q. N. Chan, G. J. Nathan, D. Roekaerts, and K. D. King, "Soot volume fraction in a piloted turbulent jet non-premixed flame of natural gas," Combustion and Flame **156**, 1339–1347 (2009).
[26] V. Narayanaswamy and N. T. Clemens, "Simultaneous LII and PIV measurements in the soot formation region of turbulent non-premixed jet flames," Proceedings of the Combustion Institute **34**, 1455–1463 (2013).
[27] N. H. Qamar, G. J. Nathan, Z. T. Alwahabi, and K. D. King, "The effect of global mixing on soot volume fraction: measurements in simple jet, precessing jet, and bluff body flames," Proceedings of the Combustion Institute **30**, 1493–1500 (2005).
[28] T. R. Meyer, S. Roy, V. M. Belovich, E. Corporan, and J. R. Gord, "Simultaneous planar laser-induced incandescence, OH planar laser-induced fluorescence, and droplet mie scattering in swirl-stabilized spray flames," Applied Optics **44**, 445–454 (2005).
[29] K. P. Geigle, M. Köhler, W. O'Loughlin, and W. Meier, "Investigation of soot formation in pressurized swirl flames by laser measurements of temperature, flame structures and soot concentrations," Proceedings of the Combustion Institute, DOI:10.1016/j.proci.2014.05.135 (posted 25 June 2014, in press).
[30] B. Franzelli, P. Scouflaire, and S. Candel, "Time-resolved spatial patterns and interactions of soot, PAH and OH in a turbulent diffusion flame," Proceedings of the Combustion Institute, DOI:10.1016/j.proci.2014.06.123 (posted 17 July 2014, in press).
[31] J. Sjöholm, R. Wellander, H. Bladh, M. Richter, P.-E. Bengtsson, M. Alden, U. Aronsson, C. Chartier, O. Andersson, and B. Johansson, "Challenges for in-cylinder high-speed two-dimensional laser-induced incandescence measurements of soot," SAE Technical Paper 2011-01-1280, SAE International, Warrendale, PA (2011).
[32] M. Köhler, I. Boxx, K. P. Geigle, and W. Meier, "Simultaneous planar measurements of soot structure and velocity fields in a turbulent lifted jet flame at 3 kHz," Applied Physics B **103**, 271–279 (2011).
[33] D. R. Snelling, K. E. Thomson, F. Liu, and G. J. Smallwood, "Comparison of LII derived soot temperature measurements with LII model predictions for soot in a laminar diffusion flame," Applied Physics B **96**, 657–669 (2009).
[34] E. Nordström, N.-E. Olofsson, J. Simonsson, J. Johnsson, H. Bladh, and P.-E. Bengtsson, "Local gas heating in sooting flames by heat transfer from laser-heated particles investigated using rotational CARS and LII," Proceedings of the Combustion Institute **35**, 3707–3713 (2015).
[35] P. P. Wu and R. B. Miles, "High-energy pulse-burst laser system for megahertz-rate flow visualization," Optics Letters **25**, 1639–1641 (2000).
[36] M. N. Slipchenko, J. D. Miller, S. Roy, J. R. Gord, S. A. Danczyk, and T. R. Meyer, "Quasi-continuous burst-mode laser for high-speed planar imaging," Optics Letters **37**, 1346–1348 (2012).
[37] F. Fuest, M. J. Papageorge, W. R. Lempert, and J. A. Sutton, "Ultrahigh laser pulse energy and power generation at 10 kHz," Optics Letters **37**, 3231–3233 (2012).
[38] J. B. Michael, P. Venkateswaran, J. D. Miller, M. N. Slipchenko, J. R. Gord, S. Roy, and T. R. Meyer, "100??kHz thousand-frame burst-mode planar imaging in turbulent flames," Optics Letters **39**, 739–742 (2014).
[39] M. N. Slipchenko, J. D. Miller, S. Roy, T. R. Meyer, J. G. Mance, and J. R. Gord, "100 kHz, 100 ms, 400 j burst-mode laser with dual-wavelength diode-pumped amplifiers," Optics Letters **39**, 4735 (2014).
[40] B. Böhm, C. Heeger, R. L. Gordon, and A. Dreizler, "New perspectives on turbulent combustion: Multi-parameter high-speed planar laser diagnostics," Flow, Turbulence and Combustion **86**, 313–341 (2011).

[41] N. Jiang, M. Webster, W. R. Lempert, J. D. Miller, T. R. Meyer, C. B. Ivey, and P. M. Danehy, "MHz-rate nitric oxide planar laser-induced fluorescence imaging in a mach 10 hypersonic wind tunnel," Applied Optics **50**, A20 (2011).
[42] K. N. Gabet, R. A. Patton, N. Jiang, W. R. Lempert, and J. A. Sutton, "High-speed CH2o PLIF imaging in turbulent flames using a pulse-burst laser system," Applied Physics B **106**, 569–575 (2012).
[43] M. J. Papageorge, T. A. McManus, F. Fuest, and J. A. Sutton, "Recent advances in high-speed planar rayleigh scattering in turbulent jets and flames: increased record lengths, acquisition rates, and image quality," Applied Physics B **115**, 197–213 (2014).
[44] J. D. Miller, J. B. Michael, M. N. Slipchenko, S. Roy, T. R. Meyer, and J. R. Gord, "Simultaneous high-speed planar imaging of mixture fraction and velocity using a burst-mode laser," Applied Physics B **113**, 93–97 (2013).
[45] M. J. Papageorge and J. A. Sutton, "Simultaneous high-resolution kHz-rate 2-d conserved scalar and 3- component velocity field measurements in gas-phase turbulent jets," (Lisbon, Portugal, 2014).
[46] B. Thurow, N. Jiang, and W. Lempert, "Review of ultra-high repetition rate laser diagnostics for fluid dynamic measurements," Measurement Science and Technology **24**, 012002 (2013).
[47] Edgewave GmbH, "Edgewave IS series data sheet," http://www.edge-wave.de/web/en/produkte/short-pulse-systeme/is-serie/ (accessed Oct. 2014).
[48] R. J. Santoro, H. G. Semerjian, and R. A. Dobbins, "Soot particle measurements in diffusion flames," Combustion and Flame **51**, 203–218 (1983).
[49] J. Zhang, C. R. Shaddix, and R. W. Schefer, "Design of model-friendly turbulent non-premixed jet burners for C2+ hydrocarbon fuels," Review of Scientific Instruments **82**, 074101 (2011).
[50] R. J. Santoro, T. T. Yeh, J. J. Horvath, and H. G. Semerjian, "The transport and growth of soot particles in laminar diffusion flames," Combustion Science and Technology **53**, 89–115 (1987).